

¹A. Zadauly, ²A.O. Beketaeva

¹Institute of Mechanics and Engineering Science, Kazakhstan, Almaty

²Institute of Mathematics and Mathematical Modeling, Kazakhstan, Almaty,
e-mail: akerkeh_333@mail.ru

**NUMERICAL SIMULATION
OF A SUPERSONIC TURBULENT COMPRESSIBLE JET
IN A CO-FLOW WITH STOCHASTIC
SPECTRAL INFLOW BOUNDARY CONDITIONS**

Abstract. A compressible supersonic turbulent jet of a perfect gas in a co-flow with the formulation of stochastic spectral inflow boundary conditions is numerically modeled. The base equations are the LES averaged Navier – Stokes equations closed by the Smagorinsky model, the solution of which is carried out by the ENO scheme of the third order of accuracy. The stochastic boundary conditions at the inlet are constructed on the basis of the spectral method of generating fluctuations of gas-dynamic variables to obtain an inhomogeneous anisotropic turbulent flow. The numerical results of turbulent characteristics are compared with experimental data for the shear layer problem. The thickness of the shear layer is obtained, in which the growth of the shear layer between the jet and the co-flow for three types of grid (coarse, medium and fine) is demonstrated. Coherent vortex structures appearing in the jet are constructed in dynamics, which made it possible to analyze in detail the growth and development of vortices over time.

Key words: supersonic jet, supersonic co-flow, LES, spectral boundary conditions, shear layer.

Introduction

Turbulent jet flows are of particular interest when considering many aerodynamic problems, such as turbulent mixing of a jet of fuel with co-flowing air in rocket combustion chambers, predicting the noise level of propulsion systems, the interaction of jets when launching space rocket technology with launch equipment. Turbulent jets were experimentally studied in the works of many authors [1-7,25]. The issue of numerical simulation of such flows is especially relevant today, and the application of the LES method (large eddy simulation) is justified, since it gives a more accurate description of turbulence, while, in contrast to the direct numerical simulation (DNS), without requiring large computational resources. The main problem of the LES method is the correct formulation of the inflow boundary conditions. Stochastic spectral boundary conditions are promising for this method, since they give the result closest to reality and do not require a large amount of information about the statistics of turbulent characteristics. The spectral boundary conditions use a set of random numbers that satisfies the given statistical turbulence data [8–13], and the key point

in their formulation is the introduction of an anisotropic perturbation field. The ways of introducing anisotropy and inhomogeneity in the velocity field lead to a similarity between turbulence obtained numerically and natural real turbulence. In [14], using the spectral boundary conditions, an inhomogeneous anisotropic field of turbulence velocities with zero divergence was synthesized for a plane turbulent flow in a channel and for a circulation flow, and as a result, turbulent structures in the flow close to the real ones were obtained. In many works, spectral boundary conditions were used to solve actual physical problems, as, for example, in [15] the effect of wind on a tall steel building was studied. The authors found that the velocity profiles of the incoming wind flow mainly affect the average pressure coefficients of the building and the profiles of random turbulent intensities significantly affect the fluctuation forces of the wind. In [16], a comparison was made between the LES models with different boundary conditions, including spectral ones, as well as a comparison with experiment in order to determine the accuracy of the LES method when simulating flows in combustion chambers, using the example of particle distribution in circulating two-phase flows.

As a result, the authors simulated the characteristic fluctuation velocity fields, which gave a satisfactory agreement with the experiment. The authors of [17] studied the spread of atmospheric pollution on the streets of the city by modeling atmospheric flows with a boundary layer with obstacles. The study was conducted numerically using the RANS model and the LES model with spectral boundary conditions. Both methods were compared with each other and with experimental data. As a result, the LES method was able to detect both external and internal induced periodicities and, accordingly, pulsating and unstable fluctuations in the flow field, which made it possible to obtain the correct calculation of the transient process of mixing air with a pollutant using the example of city streets. This in turn led to a more accurate prediction of horizontal concentration diffusion, since it was the LES method with spectral boundary conditions that made it possible to reproduce unsteady concentration fluctuations. In [18], using the LES, turbulent combustion of methane and oxygen with preliminary mixing was simulated using spectral boundary conditions, a comparison was made with experiment, and a satisfactory agreement between the numerical and

experimental calculations was obtained. The authors of [19] investigated the effect of oncoming turbulent structures in the air flow on the low-speed wing. Good results were obtained from the wing response to the effects of turbulent structures in both two-dimensional and three-dimensional modeling. In [20], a turbulent flow passing through a rotating wind turbine was simulated using the LES with spectral boundary conditions in order to study the formation and propagation of a wake behind a wind turbine. As a result, the structures obtained behind the wind turbine turned out to be a system of intense and stable rotating spiral vortices, which determined the dynamics of the wake. As a recommendation, the authors proposed the following: the boundary between the near and far wake should be defined as the initial location for the decay of the wake. Also, a comparison with experiment was made in the work, which gave good agreement on the time-averaged pressure coefficients.

The aim of this work is numerical simulation of a supersonic turbulent jet of a perfect gas in a co-flowing air stream using the LES method with stochastic spectral boundary conditions at the input. The schematic flow diagram is presented in Figure 1:

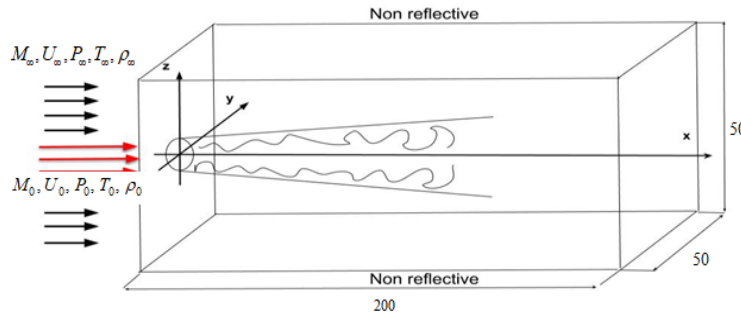


Figure 1 – Schematic flow diagram

Basic equations

The basic equations are a system of three-dimensional LES-filtered Navier-Stokes equations for a compressible turbulent perfect gas in a Cartesian coordinate system, written in a conservative form:

$$\frac{\partial \vec{U}}{\partial t} + \frac{\partial (\vec{E} - \vec{E}_v)}{\partial x} + \frac{\partial (\vec{F} - \vec{F}_v)}{\partial y} + \frac{\partial (\vec{G} - \vec{G}_v)}{\partial z} = 0 \quad (1)$$

where vectors of dependent parameters and vectors of flow are defined as:

$$\begin{aligned} \vec{U} &= (\rho, \rho u, \rho v, \rho w, E_t)^T \\ \vec{E} &= (\rho u, \rho u^2 + P, \rho uv, \rho uw, (E_t + P)u)^T \\ \vec{F} &= (\rho v, \rho uv, \rho v^2 + P, \rho vw, (E_t + P)v)^T \\ \vec{G} &= (\rho w, \rho uw, \rho vw, \rho w^2 + P, (E_t + P)w)^T \\ \vec{E}_v &= (0, \tau_{xx}, \tau_{xy}, \tau_{xz}, u\tau_{xx} + v\tau_{xy} + w\tau_{xz} - q_x)^T \\ \vec{F}_v &= (0, \tau_{xy}, \tau_{yy}, \tau_{yz}, u\tau_{xy} + v\tau_{yy} + w\tau_{yz} - q_y)^T \\ \vec{G}_v &= (0, \tau_{xz}, \tau_{yz}, \tau_{zz}, u\tau_{xz} + v\tau_{yz} + w\tau_{zz} - q_z)^T \end{aligned}$$

The components of the viscous stress tensor are defined as follows:

$$\begin{aligned}\tau_{xx} &= \frac{2\mu_{eff}}{3Re} (2u_x - v_y - w_z) \\ \tau_{yy} &= \frac{2\mu_{eff}}{3Re} (2v_y - u_x - w_z) \\ \tau_{zz} &= \frac{2\mu_{eff}}{3Re} (2w_z - u_x - v_y) \\ \tau_{xy} &= \tau_{yx} = \frac{\mu_{eff}}{Re} (u_y + v_x) \\ \tau_{xz} &= \tau_{zx} = \frac{\mu_{eff}}{Re} (u_z + w_x) \\ \tau_{yz} &= \tau_{zy} = \frac{\mu_{eff}}{Re} (v_z + w_y)\end{aligned}$$

Heat flows are represented as:

$$\begin{aligned}q_x &= -\frac{\mu_{eff}}{(\gamma-1)M_\infty^2 PrRe} T_x \\ q_y &= -\frac{\mu_{eff}}{(\gamma-1)M_\infty^2 PrRe} T_y \\ q_z &= -\frac{\mu_{eff}}{(\gamma-1)M_\infty^2 PrRe} T_z\end{aligned}$$

Effective viscosity is the sum of the dynamic and vortex viscosities: $\mu_{eff} = \mu_l + \mu_{sgs}$, where μ_l is obtained from the Sutherland's formulae, and μ_{sgs} is as follows:

$$\begin{aligned}\mu_{sgs} &= \rho(C\Delta)^2 \sqrt{\tilde{S}_{ij}\tilde{S}_{ij}}, \\ \tilde{S}_{ij} &= \frac{1}{2} \left(\frac{\partial \tilde{u}_i}{\partial x_j} + \frac{\partial \tilde{u}_j}{\partial x_i} \right), i=1,2,3, j=1,2,3\end{aligned}\quad (2)$$

where C is semi-empirical coefficient of the model, $\Delta = \Delta x \cdot \Delta y \cdot \Delta z$ is the width of the filter.

Pressure and temperature are set as follows:

$$\begin{aligned}P &= (\gamma-1) \left[E_t - \frac{1}{2} (\rho u^2 + \rho v^2 + \rho w^2) \right] \\ T &= \left(\frac{1}{\rho c_v} \right) \left[E_t - \frac{1}{2} (\rho u^2 + \rho v^2 + \rho w^2) \right]\end{aligned}\quad (3)$$

$$c_v = \frac{1}{\gamma(\gamma-1)M_\infty^2}$$

In (1) u, w, v are the components of the velocity vector, ρ is the density, c_v is the specific heat at constant volume, γ is the specific heat ratio, M_∞ is the flow Mach number.

The system (1) is written in dimensionless form, where the flow parameters $u_\infty, \rho_\infty, T_\infty$ taken as a reference values; for the pressure P and the total energy E_t the reference values are $\rho_\infty u_\infty^2$, the length scale is the initial vorticity thickness of a mixing layer:

$$\delta_\theta(x) = \int_{-H/2}^{+H/2} (\bar{\rho}(\tilde{u} - u_\infty) \cdot (u_0 - \tilde{u}) / (\rho_\infty \Delta u^2)) dz$$

where $\tilde{u} = (u - u_\infty) / \Delta u$ $\Delta u = u_0 - u_\infty$

Pr, Re are the Prandtl and the Reynolds numbers. Index 0 corresponds to the parameters of the jet and index ∞ corresponds to the parameters of the flow.

Boundary and Initial conditions

At the input, the initial conditions for the velocity profile are set in the form:

$$\vec{V}(x_i, t) = \vec{V}(x_i)^{base} + \vec{V}(x_i, t)^{natural}\quad (4)$$

where $\vec{V} = (u, v, w)$, $(x_i) = (x, y, z)$

$\vec{V}(x_i)^{base}$ is the velocity field given as follows:

$$\vec{V}(x_i)^{base} = \begin{cases} u_\infty = 1, v_\infty = 0, w_\infty = 0, \\ \text{for } x = 0, 0 \leq y \leq H_y, 0 \leq z \leq H_z \\ u_0 = \sqrt{T_0} \frac{M_0}{M_\infty}, v_0 = 0, w_0 = 0, \\ \text{for } x = 0, |z^2 + y^2| \leq R \end{cases}$$

At the transition of two gas flows, the above physical variables are determined by the function of the hyperbolic tangent:

$$\phi(z) = 0.5(\phi_0 + \phi_\infty) + 0.5(\phi_0 - \phi_\infty) \tanh(0.5z / \delta_\theta) \quad (5)$$

where $\phi = (u, v, w)$.

Here H_x, H_y and H_z are length, width, and height of the computational domain, respectively, and R is the radius of the jet orifice.

The “natural” fluctuation velocity field at the entrance $\vec{V}(x_i, t)^{natural}$ from (4) is given by analogy as in [13] and the spectral boundary conditions at the entrance for this case are as follows:

$$\vec{V}(x_i, t) = 0.5 \cdot \sum_{n=1}^N \sqrt{q^n} [\cos(k^n \cdot d \cdot x_i + \varphi_n)]$$

where d is the random frequency and φ_n is the random phase shift, both determined in the interval $[0;1]$, here N is taken as $N=100$ and q^n is the normalized amplitude:

$$q^n = \frac{E(k^n) \Delta k^n}{\sum_{n=1}^N E(k^n) \Delta k^n}, \quad \sum_{n=1}^N q^n = 1$$

where $E(k)$ is the modified von Karman energy spectrum:

$$E(k) = \frac{(k/k_e)^4}{[1 + 2.4(k/k_e)^2]^{17/6}} \quad (7)$$

where

$$k^n = k^{\min} \cdot (1 + \alpha)^{n-1}, \quad n = 1 \div N, \quad \alpha = 0.01$$

$$k^{\min} = \beta \cdot k_e^{\min}, \beta \leq 1, k_e^{\min} = \frac{2\pi}{l_e^{\max}},$$

$$l_e^{\max} = \max(h_x, h_z, h_y)$$

In the output and the lateral boundaries the non reflective boundary conditions are specified [21].

Method of solution

Preliminary, at the level of the jet injection, a thickening of the grid is introduced for a more accurate numerical solution. Then the system (1) in the transformed coordinate system is written in the form:

$$\frac{\partial \tilde{U}}{\partial t} + \frac{\partial \tilde{E}}{\partial \xi} + \frac{\partial \tilde{F}}{\partial \zeta} + \frac{\partial \tilde{G}}{\partial \eta} = \frac{\partial \tilde{E}_v}{\partial \xi} + \frac{\partial \tilde{F}_v}{\partial \zeta} + \frac{\partial \tilde{G}_v}{\partial \eta} \quad (9)$$

where $\tilde{U} = \bar{U}/J, \tilde{E} = \xi_x \bar{E}/J, \tilde{F} = \zeta_y \bar{F}/J, \tilde{G} = \eta_z \bar{G}/J, \tilde{E}_v = \xi_x \bar{E}_v/J, \tilde{F}_v = \zeta_y \bar{F}_v/J, \tilde{G}_v = \eta_z \bar{G}_v/J$ и $J = \partial(\xi, \zeta, \eta) / \partial(x, y, z)$ is the Jacobian transform.

The solution of the system (9) is performed with semi-implicit method proposed in [22, 23].

Firstly, the linearization procedure is applied to the equations (9). Then, the factored scheme of the linearized system is written. This form reduced the three-dimensional matrix inversion problem to the three one-dimensional problems in directions ξ, ζ, η . Secondly, the obtained one-dimensional problems are solved implicitly with matrix sweep method for the vector \tilde{U} . Here, the advective terms are approximated using the third-order ENO scheme in detail represented by authors in [22, 23]. The central differences of the second order accuracy are used for approximation of diffusion terms.

Results

The verification of the numerical model is conducted by the comparison of the computational results with the experimental data of [24] for the shear layer problem. Schematic diagram of the flow is presented in Figure 2:

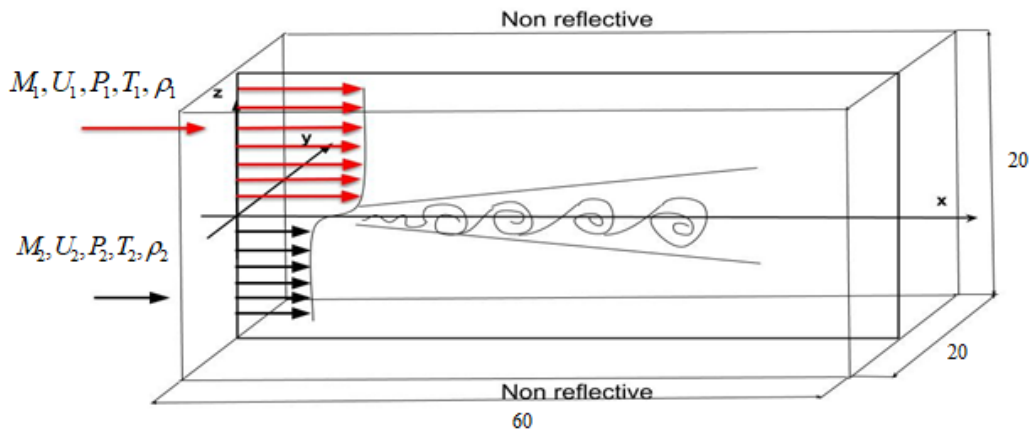


Figure 2 – Schematic diagram of the shear layer problem

Two parallel flows with different Mach numbers are defined by the following parameters:

M_1	M_2	M_c	U_1 / U_2	ρ_1 / ρ_2	T	p
1.80	0.51	0.51	0.36	0.64	291K	1 atm.

where

$M_c = (U_1 - U_c) / a_1, (a_1 U_2 + a_2 U_1) / (a_1 + a_2)$ is the convective Mach number and U_1, U_2 are velocities of the upper (indexed by 1) and lower flows (indexed by 2), and a_1, a_2 are the local sound velocities of flows. The pressure at the input remains constant. The simulation is made for three types of grids: coarse (75x25x25 nodes), middle (135x51x51 nodes), fine (271x101x101 nodes). This is made in purpose for the grid independence analysis which shows that the simulation with the computational grid of 301x131x131 nodes gives the same results as for the 271x101x101 nodes

simulations. And this is the cause why there is no need of using more computational resources with finer grid and here the grid of 271x101x101 nodes is in use. At the input, the spectral boundary conditions are used.

The results of comparing turbulent characteristics with experiment are shown in Figure 3-5 for $x = 180$ cross-section. For stream wise and lateral turbulence intensities and for Reynolds stress profiles a satisfactory agreement with experiment is obtained (grid of 271x101x101 nodes). This result confirms the validity and correctness of the selected spectral boundary conditions at the input.

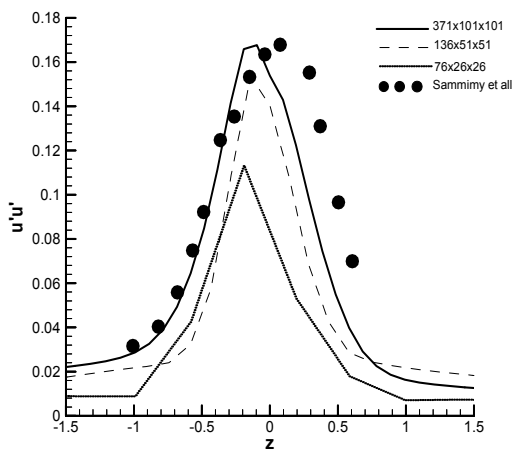


Figure 3 – Streamwise turbulence intensities

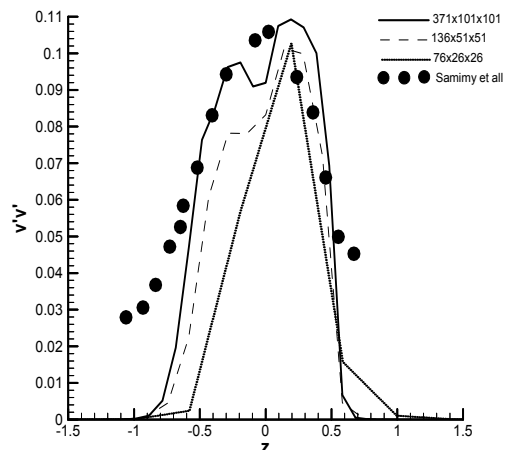


Figure 4 – Lateral turbulence intensities

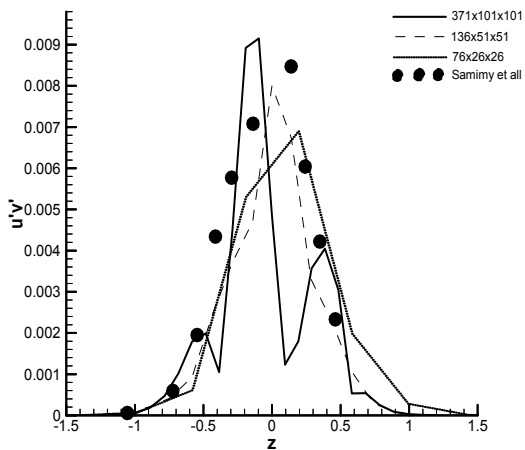


Figure 5 – The Reynolds stress profiles

The following are the results of numerical modeling of the problem with the following parameters: $M_\infty = 1$, $M_0 = 2$, $Re = 10^5$, $d = 6$ is the diameter of the orifice, $P = 1atm$ is the pressure which is constant. The sizes of the domain are next $H_x = 200$, $H_y = 200$, $H_z = 30$ and $y_0 = 25$, $z_0 = 25$ are coordinates of the center of the jet.

In Figure 6 showing the vorticity thickness

$$\delta_\omega = \frac{u_\infty - u_0}{(\partial u / \partial z)_{max}}$$

of the shear layer, shows the results of calculations with three types of grids for comparison. In the case of a fine mesh (black solid line), the vorticity thickness increases from 4.7 to 8.5.

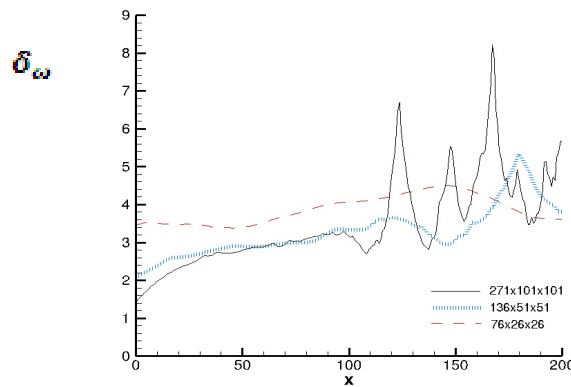


Figure 6 – Vorticity thickness for three types of grids.

Figure 7 (a) presents instantaneous isosurfaces for densities and vorticity, and Figure 7 (b) shows

isolines of density and vorticity in a cross section $y=25$ for natural jet in co-flow

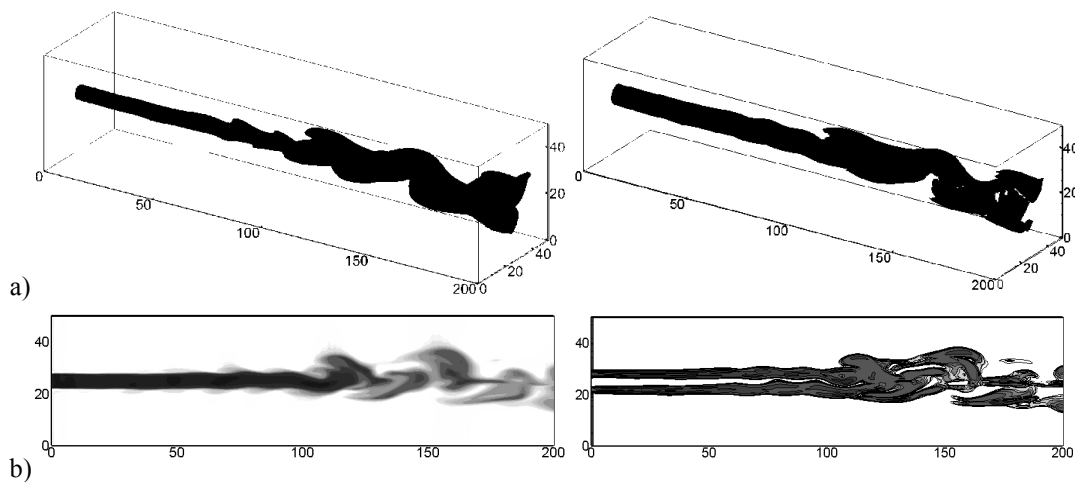


Figure 7 – Instantaneous isosurface for densities and vorticity (a), isolines of density and vorticity in cross section $y=25$ (b) for natural jet in co-flow

The results on Figure 7 show that with spectral boundary conditions taken at the input the obtained turbulence is close to the real one. As it is seen there are 6 vortices appeared starting from the point $x = 55$ which seems to be a good result for this kind of flows. The main problem in all supersonic flows is in making the starting point (where the vortices start to form) distance as

shorter as possible. Solving this problem leads to beneficial improvements in construction of the combustion chambers, namely the reduced size of combustors. More detailed analysis of the formation of vortices is shown on Figure 8 where the dynamic of the vortices structures in the shear layer between jet and co-flow is demonstrated:

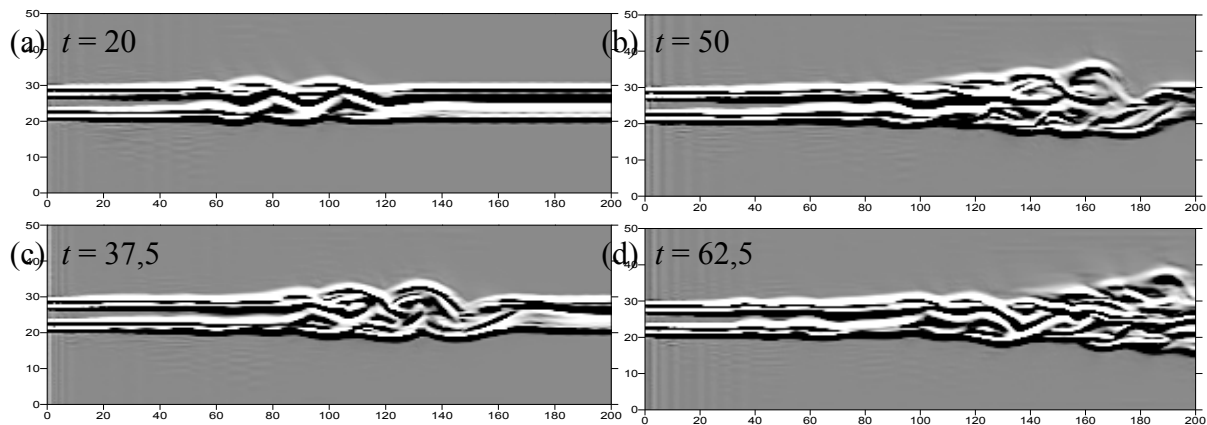


Figure 8 – Evolution of vorticity isolines at various times for natural jet in co-flow

It shows that to the time $t = 37.5$ the vortices are started forming and they are moving downstream (Fig. 8 (b)). Pairing of the adjacent vortices with forming the larger ones is demonstrated in Fig. 8 (c). And the relatively stable turbulence occurs to the time $t = 62.5$ (Fig. 8 (d)).

Conclusion

Stochastic boundary conditions at the entrance are presented based on the spectral method of generating fluctuations of gas-dynamic variables to obtain an inhomogeneous anisotropic turbulent flow. Based on them, the problem of injecting the compressible supersonic turbulent jet into a co-flowing stream is numerically solved. The analysis of grid independence for computational grids is carried out, which gave the most suitable number of nodes for the grid. Comparison of the results of obtained turbulent characteristics with experiment showed satisfactory agreement. It was also revealed that the far region of the jet in the shear layer is characterized by a developed turbulent structure. Thus, the formulation of stochastic spectral boundary conditions made it possible to obtain anisotropic inhomogeneous turbulence close to real.

References

1. M.R. Davis. Measurements in a subsonic turbulent jet using a quantitative schlieren technique // *J. Fluid Mech.* – 1971. – Vol. 46, part 4. – P. 631-656.
2. M.R. Davis. Quantitative schlieren measurements in a supersonic turbulent jet // *J. Fluid Mech.* – 1972. – Vol. 51, part 3. – P. 435-447.
3. R.A. Antonia and R.W. Bilger. An experimental investigation of an axisymmetric jet in a co-flowing air stream // *J. Fluid Mech.* – 1973. – Vol. 61, part 4. – P. 805-822.
4. J.-L. Boreau, D. Huilier, H. Burnage. On the effect of a co-flowing stream on the structure of an axisymmetric turbulent jet // *Experimental Thermal and Fluid Science.* – 1998. – Vol. 17. – P. 10-17.
5. L.P. Xia, K.M. Lam. Velocity and concentration measurements in initial region of submerged round jets in stagnant environment and in coflow // *Journal of Hydro-environment Research.* – 2009. – Vol. 3. – P. 21-34.
6. J.J. Charonko and K. Prestridge. Variable-density mixing in turbulent jets with coflow // *J. Fluid Mech.* – 2017. – Vol. 825. – P. 887-921.
7. F. De Gregorio, F. Albano. Free compressible jet nozzle investigation // *16th Int.*

Symp. on Applications of Laser Techniques to Fluid Mechanics, Lisbon, Portugal. – 9-12 July, 2012.

8. A. Smirnov, S. Shi and I. Celik. Random Flow Generation Technique for Large Eddy Simulations and Particle-Dynamics Modeling // *Journal of Fluids Engineering*. – 2001. – Vol. 123, No. 2. – P. 359–371.
9. P. Batten, U. Goldberg and S. Chakravarthy. Interfacing Statistical Turbulence Closures with Large-Eddy Simulation // *AIAA Journal*. – 2004. – Vol. 42, No. 3. – P. 485–492.
10. L. Davidson. Hybrid LES-RANS: Inlet Boundary Conditions for Flows Including Recirculation // *Proceedings of the 5th International Symposium on Turbulence and Shear Flow Phenomena*. – 2007. – Vol. 2. – P. 689–694.
11. S. Huang, Q. Li and J. Wu. A General Inflow Turbulence Generator for Large Eddy Simulation // *Journal of Wind Engineering and Industrial Aerodynamics*. – 2010. – Vol. 98, No. 10–11. – P. 600–617.
12. H.G. Castro and R.R. Paz. A Time and Space Correlated Turbulence Synthesis Method for Large Eddy Simulation // *Journal of Computational Physics*. – 2013. – Vol. 235. – P. 742–763.
13. D. Yu. Adamyant, M.H., Strelets and A.K. Travin. An efficient method of generation of synthetic turbulence at the entrance boundaries of the LES region within the framework of combined RANS-LES approaches to the calculation of turbulent flows // *Mathematical Modeling*. – 2011. – Vol. 23, No. 7. – P. 3-19.
14. R.Yu and X.-S. Bai. A Fully Divergence-Free Method for Generation of Inhomogeneous and Anisotropic Turbulence with Large Spatial Variation // *Journal of Computational Physics*. – 2014. – Vol. 256. – P. 234–253.
15. S. Huang, Q. Li and S. Xu. Numerical Evaluation of Wind Effects on a Tall Steel Building by CFD // *Journal of Constructional Steel Research*. – 2007. – Vol. 63, No. 5. – P. 612–627.
16. E. Riber, V. Moureau, M. Garcia, T. Poinso and O. Simonin. Evaluation of Numerical Strategies for Large Eddy Simulation of Particulate Two-Phase Recirculating Flows // *Journal of Computational Physics*. – 2009. – Vol. 228, No. 2. – P. 539–564.
17. S. M. Salim, R. Buccolieri, A. Chan and S.D. Sabatino. Numerical Simulation of Atmospheric Pollutant Dispersion in an Urban Street Canyon: Comparison Between RANS and LES // *Journal of Wind Engineering and Industrial Aerodynamics*. – 2011. – Vol. 99, No. 2–3. – P.103–113.
18. G. Wang, M. Boileau and D.Veynante. Implementation of a Dynamic Thickened Flame Model for Large Eddy Simulations of Turbulent Premixed Combustion // *Combustion and Flame*. – 2011. – Vol. 158, No. 11. – P. 2199–2213.
19. V. Golubev, J. Brodnick, L. Nguyen, J. Dudley and M. Visbal. High-Fidelity Simulations of Airfoil Interaction with Upstream Turbulence // 42nd AIAA Fluid Dynamics Conference and Exhibit, AIAA Paper 2012-3071. – June 2012.
20. J. Mo, A. Choudhry, M. Arjomandi and Y. Lee. Large Eddy Simulation of the Wind Turbine Wake Characteristics in the Numerical Wind Tunnel Model // *Journal of Wind Engineering and Industrial Aerodynamics*. – 2013. – Vol. 112. – P. 11–24.
21. T.J. Poinso, S.K. Lele. Boundary Conditions for Direct Simulation of Compressible Viscous Flows // *Journal of Computational Physics*. – 1992. – Vol. 101. – P.104-129.
22. A. Beketaeva, A. Naimanova. Flow structure of the transverse jet interaction with supersonic flow for moderate to high pressure ratios // *International journal of mechanics*. – 2018. – Vol.12. – P. 88-95.
23. A. Beketaeva, P. Bruel and A. Naimanova. Vortical structures behind a transverse jet in a supersonic flow at high jet to crossflow pressure ratios // *J. Appl. Mech. and Tech. Phys.* – 2015. – Vol. 56, No 5. – P. 777-788.
24. M. Samimy and G.S. Elliott. Effects of compressibility on the characteristics of free shear layers // *AIAA Journal*. – 1990. – Vol. 28, No. 3. – P. 439-445.
25. A. Zadauly, A. Beketaeva Influence of slit sizes on the interaction structure of supersonic turbulent air flow with a multi-component injection jet in a channel // *International Journal of Mathematics and Physics* – 2018 – V.9, № 2. – P.72-85.